

Crossover from bias-induced to field-induced breakdowns in one-dimensional band and Mott insulators attached to electrodes

Yasuhiro Tanaka* and Kenji Yonemitsu

Institute for Molecular Science, Okazaki 444-8585, Japan

Department of Functional Molecular Science, Graduate University for Advanced Studies, Okazaki 444-8585, Japan and JST, CREST, Sanbancho, Chiyoda-ku, Tokyo 102-0075, Japan

(Dated: February 26, 2018)

Nonequilibrium states induced by an applied bias voltage (V) and the corresponding current-voltage characteristics of one-dimensional models describing band and Mott insulators are investigated theoretically by using nonequilibrium Green's functions. We attach the models to metallic electrodes whose effects are incorporated into the self-energy. Modulation of the electron density and the scalar potential coming from the additional long-range interaction are calculated self-consistently within the Hartree approximation. For both models of band and Mott insulators with length L_C , the bias voltage induces a breakdown of the insulating state, whose threshold shows a crossover depending on L_C . It is determined basically by the bias $V_{th} \sim \Delta$ for L_C smaller than the correlation length $\xi = W/\Delta$ where W denotes the bandwidth and Δ the energy gap. For systems with $L_C \gg \xi$, the threshold is governed by the electric field, V_{th}/L_C , which is consistent with a Landau-Zener-type breakdown, $V_{th}/L_C \propto \Delta^2/W$. We demonstrate that the spatial dependence of the scalar potential is crucially important for this crossover by showing the case without the scalar potential, where the breakdown occurs at $V_{th} \sim \Delta$ regardless of the length L_C .

PACS numbers: 77.22.Jp, 73.40.Rw, 71.10.Fd, 72.20.Ht

I. INTRODUCTION

Nonlinear conduction in correlated electron systems such as one-dimensional Mott insulators^{1,2} and two-dimensional charge-ordered materials³⁻⁸ has been of great interest in the past few decades. They offer intriguing subjects of nonequilibrium physics in condensed matter and possibility for novel functions of electronic devices. For example, in a typical quasi-one-dimensional Mott insulator, Sr_2CuO_3 ,¹ a dielectric breakdown has been observed experimentally by applying a strong electric field. A dielectric breakdown has been reported also in an organic spin-Peierls insulator, K-TCNQ² [TCNQ=tetracyanoquinodimethane]. For another organic compound, (BEDT-TTF)(F₂TCNQ) [BEDT-TTF=bis(ethylenedithio)tetrathiafulvalene], which is a quasi-one-dimensional Mott insulator, metal-insulator-semiconductor field-effect transistor device structures have been reported,⁹ where its field-effect characteristics are different from those of band insulators.¹⁰⁻¹²

So far, theoretical investigations on nonlinear conduction for interacting electron systems that are initially insulating in their equilibrium states have been done by several authors.¹⁰⁻²² In general, these studies are classified into two approaches depending on whether an external force is written as an electric field^{13,14,16-19} or a bias voltage.^{10-12,15,20-22} The former approach is to consider electron systems without electrodes. The electric field is usually applied with open boundary condition,¹⁴ or equivalently with periodic boundary condition by using a time-dependent magnetic flux.^{13,16} In one dimension, Oka and Aoki studied the Hubbard model under a strong electric field by the time-dependent density-matrix-renormalization-group method.¹⁴ One of their im-

portant results is that the dielectric breakdown of Mott insulators is interpreted as a many-body counterpart of the Landau-Zener (LZ) breakdown.^{23,24} This is known to describe the breakdown of band insulators where the one-particle picture holds. The threshold is given as $E_{th} \propto \Delta^2$ with Δ being an energy gap. A mean-field approach to electric-field-induced insulator-to-metal transitions by using Keldysh Green's functions has been reported in Ref. 19.

The latter approach is to consider an insulator attached to electrodes. Interface structures must be explicitly taken into account in real electric devices. Along this line, Okamoto investigated the current-voltage (I - V) characteristics of heterostructures that consist of Mott-insulator layers sandwiched by metallic leads by combining the dynamical mean-field theory with the Keldysh Green's function technique.^{20,21} Ajisaka *et al.* studied the I - V characteristics of an electron-phonon system coupled with two reservoirs by a field-theoretical method.²² In the studies listed above, Okamoto discussed the I - V characteristics in the framework of the LZ breakdown, while Ajisaka *et al.* proposed a different mechanism with the threshold bias voltage $V_{th} \sim \Delta$. These results seem to be inconsistent with each other.

When we consider a nanostructure in which some material is attached to left and right metallic electrodes, the bias voltage V applied to the material is described as $V = \mu_L - \mu_R$ with μ_L and μ_R being the chemical potentials of the left and right electrodes, respectively. Here we assume that the work-function difference at the interfaces is absent for simplicity. In this case, one might expect that the current flows when some energy levels of the material appear in the region between μ_L and μ_R , indicating the threshold governed by the applied bias voltage

$V_{\text{th}} \sim \Delta$. In fact, for the transport in a field-effect transistor with a small channel, such an explanation has been used frequently.²⁵ However, for a bulk insulator with an energy gap Δ , this picture does not hold and should be replaced by the LZ mechanism where the threshold is determined by the electric field, $E_{\text{th}} \propto \Delta^2$. This consideration poses us a question about which parameter determines the mechanism of the breakdown. In particular, we address the condition for the realization of the LZ breakdown in a structure with electrodes. It is also important to know the relation between the approaches using the structure with electrodes and those which do not include them explicitly. We point out that the size of an insulator as well as the potential distribution inside it determine the nature of the breakdown.

In this paper, we study one-dimensional band and Mott insulators attached to two electrodes (see Fig. 1), using the nonequilibrium Green's function approach that has previously been used to discuss the suppression of rectification at metal-Mott-insulator interfaces.¹² This approach more naturally describes nonequilibrium steady states than the approach based on the time-dependent Schrödinger equation because a current oscillation is inevitable in the latter owing to finite-size effects. The present method can be easily applied to higher-dimensional systems. Preliminary results for the I - V characteristics of two-dimensional charge-ordered systems are reported in Ref. 26.

We show that the applied bias voltage V induces a breakdown of band and Mott insulators at zero temperature. For both insulators, the threshold shows a crossover as a function of the size of the insulating region L_C . For systems with L_C smaller than the correlation length ξ , i.e., the characteristic decay length of the wave function in the insulator, the breakdown takes place when the bias V exceeds the energy gap Δ . For $L_C \gg \xi$, it is governed by the electric field, V/L_C , which is consistent with the LZ tunneling mechanism. Whether the charge gap is produced by the band structure or by the electron-electron interaction is irrelevant to the crossover phenomenon. We will focus on the spatial modulation of the wave functions. For the crossover behavior and the deformation of the wave functions, the spatial dependence of the scalar potential inside the band or Mott insulator is important. This is demonstrated in the Appendix by showing the case without the scalar potential, where the bias-induced transition occurs at $V_{\text{th}} \sim \Delta$ regardless of the length L_C .

II. MODEL AND FORMULATION

We consider a one-dimensional insulator that is attached to semi-infinite metallic electrodes on the left and right sides as shown in Fig. 1. The insulator is referred to as the central part, and described by the Hubbard model for a Mott insulator and a tight-binding model with alternating transfer integrals for a band insulator, both at

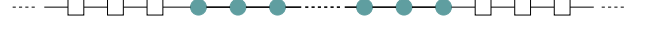


FIG. 1: (Color online) Schematic view of the model. A one-dimensional band or Mott insulator in the central part is connected by left and right electrodes. Solid (open) symbols represent the sites in the central part (electrodes).

half filling:

$$\begin{aligned}
 H = & - \sum_{i=1}^{L_C-1} \sum_{\sigma} [t + (-1)^{i-1} \delta t] (c_{i\sigma}^{\dagger} c_{i+1\sigma} + h.c.) \\
 & + U \sum_i (n_{i\uparrow} - \frac{1}{2})(n_{i\downarrow} - \frac{1}{2}) \\
 & + \sum_{\langle\langle ij \rangle\rangle} V_{ij} (n_i - 1)(n_j - 1), \quad (1)
 \end{aligned}$$

where $c_{i\sigma}^{\dagger} (c_{i\sigma})$ denotes the creation (annihilation) operator for an electron with spin σ at the i th site, $n_{i\sigma} = c_{i\sigma}^{\dagger} c_{i\sigma}$, and $n_i = n_{i\uparrow} + n_{i\downarrow}$. L_C is the total number of sites in the central part. The parameter t denotes the transfer integral, δt its modulation, and U the on-site interaction. We use t as a unit of energy. For $\delta t = 0$ and $U > 0$, the first and second terms in Eq. (1) become the one-dimensional repulsive Hubbard model, whereas they describe a band insulator for $\delta t \neq 0$ and $U = 0$. The long-range Coulomb interaction term with $V_{ij} = V_p/|i - j|$ is introduced because it is responsible for the potential modulation near the metal-insulator interfaces ($i \gtrsim 1$ and $i \lesssim L_C$). The V_{ij} term is treated by the Hartree approximation, which is equivalent to the introduction of a scalar potential that satisfies the Poisson equation. Here $\langle\langle ij \rangle\rangle$ means the summation over pairs of the i th and j th sites with $i \neq j$ in the central part ($1 \leq i, j \leq L_C$). We briefly review our formulation¹² below to treat steady states with a finite voltage.

For the metallic electrodes, we consider noninteracting electrons. The effects of the left and right ($\alpha = L, R$) electrodes on the central part are then described by the retarded self-energies.²⁷⁻²⁹ For simplicity, we take the wide-band limit so that the self-energies are independent of energy. In the present case, they become diagonal matrices²⁹

$$(\Sigma_{\alpha}^r)_{ij} = -\frac{i}{2}(\Gamma_{\alpha})_{ij} = -\frac{i}{2}\gamma_{\alpha}\delta_{ii_{\alpha}}\delta_{jj_{\alpha}}, \quad (2)$$

where $\delta_{ii_{\alpha}}$ and $\delta_{jj_{\alpha}}$ are the Kronecker delta and $i_L = 1$ ($i_R = L_C$) denotes the site connected with the left (right) electrode. We consider the case of $\gamma_L = \gamma_R$. Within the Hartree-Fock approximation for the on-site term in Eq. (1), the retarded Green's function for spin σ is written as

$$[G_{\sigma}^r(\epsilon)^{-1}]_{ij} = \epsilon\delta_{ij} - (H_{\text{HF}\sigma}^r)_{ij}, \quad (3)$$

with

$$(H_{\text{HF}\sigma}^r)_{ij} = (H_{\text{HF}\sigma})_{ij} + \sum_{\alpha=L,R} (\Sigma_\alpha^r)_{ij}. \quad (4)$$

The off-diagonal elements of $(H_{\text{HF}\sigma})_{ij}$ come from the first term of Eq. (1) and the diagonal elements are written as

$$(H_{\text{HF}\sigma})_{ii} = \psi_i + U\langle n_{i\bar{\sigma}} - 1/2 \rangle, \quad (5)$$

with $\bar{\sigma} = -\sigma$. Here, the scalar potential ψ_i is defined by the Hartree approximation to the long-range Coulomb interaction as

$$\psi_i = \sum_{j \neq i} V_{ij}(\langle n_j \rangle - 1) + ai + b, \quad (6)$$

with a and b being constants. These constants are so determined that ψ satisfies the boundary conditions:

$$\psi_i = \begin{cases} \frac{V}{2} & \text{for } i = 1 \\ -\frac{V}{2} & \text{for } i = L_C, \end{cases} \quad (7)$$

for the bias voltage V . When V is positive, the left electrode has a higher potential for the electrons and the current flows from left to right.¹² Here we assume that the work-function difference is absent at the interfaces. By diagonalizing the complex symmetric matrix $H_{\text{HF}\sigma}^r$, the retarded Green's function is obtained as

$$[G_\sigma^r(\epsilon)]_{ij} = \sum_m \frac{u_m^\sigma(i)u_m^\sigma(j)}{\epsilon - E_m^\sigma}, \quad (8)$$

where $E_m^\sigma \equiv \epsilon_m^\sigma - i\gamma_m^\sigma/2$ (ϵ_m^σ and γ_m^σ are real) is the eigenvalue of $H_{\text{HF}\sigma}^r$ and $u_m^\sigma(i)$ is the corresponding right eigenvector.

The electron density is calculated by decomposing it into the “equilibrium” and “nonequilibrium” parts¹² as

$$\langle n_{i\sigma} \rangle = n_{i\sigma}^{\text{eq}} + \sum_\alpha \delta n_{i\sigma}^\alpha. \quad (9)$$

The “equilibrium” part is defined by integrating the local density of states as

$$n_{i\sigma}^{\text{eq}} \equiv -\frac{1}{\pi} \int_{-\infty}^{\infty} d\epsilon [G_\sigma^r(\epsilon)]_{ii} f_C(\epsilon), \quad (10)$$

where $f_C(\epsilon) = \theta(\mu_C - \epsilon)$ is the Fermi distribution function with the chemical potential μ_C at the midpoint of the right and left chemical potentials, $\mu_C = (\mu_R + \mu_L)/2$. Since $\mu_L = V/2$ and $\mu_R = -V/2$, we have $\mu_C = 0$. For $V > 0$, where the left chemical potential is higher than the right, $\delta n_{i\sigma}^L$ ($\delta n_{i\sigma}^R$) is interpreted as the inflow (outflow).

The “nonequilibrium” part of the density $\delta n_{i\sigma}^\alpha$ is obtained from the “nonequilibrium” part of the lesser Green's function:

$$\delta n_{i\sigma}^\alpha \equiv \int_{-\infty}^{\infty} d\epsilon [\delta G_\sigma^{<\alpha}(\epsilon)]_{ii}. \quad (11)$$

In order to obtain $\delta G_\sigma^{<\alpha}(\epsilon)$, we first decompose the lesser self-energy in the wide-band limit²⁹ as in Eq. (9):

$$\begin{aligned} \Sigma_\sigma^{<}(\epsilon) &= i(\Gamma_L f_L(\epsilon) + \Gamma_R f_R(\epsilon)) \\ &= \Sigma_\sigma^{<\text{eq}}(\epsilon) + \sum_\alpha \delta \Sigma_\sigma^{<\alpha}(\epsilon), \end{aligned} \quad (12)$$

with

$$\Sigma_\sigma^{<\text{eq}}(\epsilon) = i(\Gamma_L + \Gamma_R) f_C(\epsilon), \quad (13)$$

and

$$\delta \Sigma_\sigma^{<\alpha}(\epsilon) = i\Gamma_\alpha [f_\alpha(\epsilon) - f_C(\epsilon)], \quad (14)$$

where $f_\alpha(\epsilon) = \theta(\mu_\alpha - \epsilon)$. Then, we employ the Keldysh equation

$$\delta G_\sigma^{<\alpha}(\epsilon) = G_\sigma^r(\epsilon) \delta \Sigma_\sigma^{<\alpha}(\epsilon) G_\sigma^a(\epsilon), \quad (15)$$

where $G_\sigma^a(\epsilon)$ is the Hermitian conjugate of $G_\sigma^r(\epsilon)$. The expressions for $n_{i\sigma}^{\text{eq}}$ and $\delta n_{i\sigma}^\alpha$, with which the numerical calculations are carried out, are obtained by substituting Eq. (8) into Eqs. (10) and (11). The results are

$$n_{i\sigma}^{\text{eq}} = \sum_m \text{Re}[u_m^\sigma(i)]^2 \left[\frac{1}{\pi} \tan^{-1} \frac{2(\mu_C - \epsilon_m^\sigma)}{\gamma_m^\sigma} + \frac{1}{2} \right], \quad (16)$$

and

$$\begin{aligned} \delta n_{i\sigma}^\alpha &= \frac{\gamma_\alpha}{2\pi} \int_{-\infty}^{\infty} d\epsilon |[G_\sigma^r(\epsilon)]_{ii_\alpha}|^2 [f_\alpha(\epsilon) - f_C(\epsilon)] \\ &= \frac{\gamma_\alpha}{2\pi} \sum_{n,m} \left\{ \text{Im} \left[\frac{u_m^\sigma(i)u_m^\sigma(i_\alpha)u_n^{*\sigma}(i)u_n^{*\sigma}(i_\alpha)}{\epsilon_m^\sigma - \epsilon_n^\sigma - i\gamma_m^\sigma/2 - i\gamma_n^\sigma/2} \right] \right\} \\ &\quad \times \left[\tan^{-1} \frac{2(\mu_\alpha - \epsilon_m^\sigma)}{\gamma_m^\sigma} - \tan^{-1} \frac{2(\mu_C - \epsilon_m^\sigma)}{\gamma_m^\sigma} \right. \\ &\quad \left. + \tan^{-1} \frac{2(\mu_\alpha - \epsilon_n^\sigma)}{\gamma_n^\sigma} - \tan^{-1} \frac{2(\mu_C - \epsilon_n^\sigma)}{\gamma_n^\sigma} \right] \\ &\quad + \text{Re} \left[\frac{u_m^\sigma(i)u_m^\sigma(i_\alpha)u_n^{*\sigma}(i)u_n^{*\sigma}(i_\alpha)}{\epsilon_m^\sigma - \epsilon_n^\sigma - i\gamma_m^\sigma/2 - i\gamma_n^\sigma/2} \right] \\ &\quad \times \left[\frac{1}{2} \ln \frac{(\mu_\alpha - \epsilon_m^\sigma)^2 + (\gamma_m^\sigma/2)^2}{(\mu_C - \epsilon_m^\sigma)^2 + (\gamma_m^\sigma/2)^2} \right. \\ &\quad \left. - \frac{1}{2} \ln \frac{(\mu_\alpha - \epsilon_n^\sigma)^2 + (\gamma_n^\sigma/2)^2}{(\mu_C - \epsilon_n^\sigma)^2 + (\gamma_n^\sigma/2)^2} \right]. \end{aligned} \quad (17)$$

In the above equations, we recover the electron density in the equilibrium state without the electrodes if $\gamma_m^\sigma = 0$, since the bracket in Eq. (16) is reduced to the step function and $\delta n_{i\sigma}^\alpha = 0$.

The current from the left electrode is expressed by the “nonequilibrium” part of the density as^{12,30}

$$\begin{aligned} J &= \int_{-\infty}^{\infty} \frac{d\epsilon}{2\pi} \sum_\sigma \text{Tr}[\Gamma_L G_\sigma^r(\epsilon) \Gamma_R G_\sigma^a(\epsilon)] [f_L(\epsilon) - f_R(\epsilon)] \\ &= \frac{\gamma_L \gamma_R}{2\pi} \int_{-\infty}^{\infty} d\epsilon \sum_\sigma |[G_\sigma^r(\epsilon)]_{i_L i_R}|^2 [f_L(\epsilon) - f_R(\epsilon)] \\ &= \gamma_R \sum_\sigma \delta n_{i_R \sigma}^L - \gamma_L \sum_\sigma \delta n_{i_L \sigma}^R, \end{aligned} \quad (18)$$

where we set $e = \hbar = 1$.

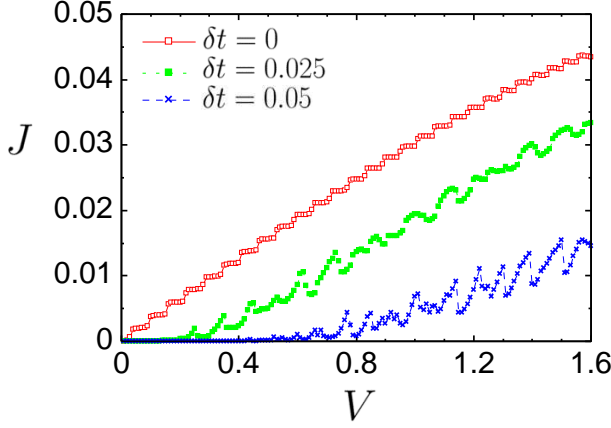


FIG. 2: (Color online) I - V characteristics of one-dimensional band insulators for $\delta t = 0.025$ and $\delta t = 0.05$. The other parameters are $L_C = 200$, $U = 0$, $V_p = 0.1$, and $\gamma_L = \gamma_R = 0.1$. Results for $\delta t = 0$ are also shown where we set $L_C = 200$, $U = 0$, $V_p = 0$, and $\gamma_L = \gamma_R = 0.1$.

III. RESULTS

In this section, we show the results of I - V characteristics, charge densities, and the spatial dependence of wave functions for band and Mott insulators. For both models, a breakdown of the insulating state takes place when the bias V becomes sufficiently large. The threshold shows a crossover behavior as a function of the size of the central part L_C , which indicates the mechanism of the breakdown changes according to L_C . The profile of the scalar potential ψ_i has crucial importance on the way of the breakdown. This is demonstrated in the Appendix by showing that, if ψ_i is artificially set to zero for all i , the crossover phenomenon disappears.

A. Band insulators

Figure 2 shows the I - V characteristics for band insulators with $\delta t = 0.025$ and 0.05 . The other parameters are $L_C = 200$, $U = 0$, $V_p = 0.1$, and $\gamma_L = \gamma_R = 0.1$. For comparison, we show the results for the regular transfer integrals ($\delta t = 0$) with $L_C = 200$, $U = 0$, $V_p = 0$, and $\gamma_L = \gamma_R = 0.1$. For $\delta t = 0$, the current J becomes nonzero for $V \neq 0$ since the central part is metallic. The I - V curve has stepwise structures owing to the finite-size effect. For $V = 0$ and $\delta t > 0$, the central part is a band insulator with the energy gap $\Delta = 4\delta t$. Because of the gap, J is suppressed near $V = 0$. The I - V curves for finite δt show more complex structures than that for $\delta t = 0$. Apart from the fine structures, J increases almost linearly for large V , which indicates a breakdown of the band insulator.

For finite voltages applied, the charge distributions in resistive and conductive states for $\delta t = 0.025$ are shown in Figs. 3 and 4, respectively. In Fig. 3(a), the elec-

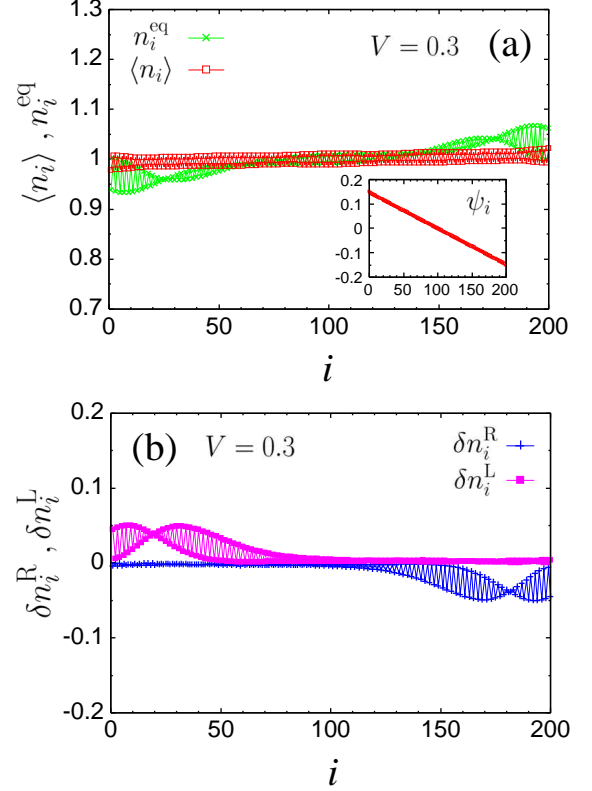


FIG. 3: (Color online) (a) Electron density, $\langle n_i \rangle$, “equilibrium” part, n_i^{eq} , and (b) “nonequilibrium” parts δn_i^R and δn_i^L for $\delta t = 0.025$, $L_C = 200$, $U = 0$, $V_p = 0.1$, $\gamma_L = \gamma_R = 0.1$, and $V = 0.3$. The scalar potential ψ_i is shown in the inset of (a).

tron density $\langle n_i \rangle = \langle n_{i\uparrow} \rangle + \langle n_{i\downarrow} \rangle$ and its “equilibrium” part $n_i^{\text{eq}} = n_{i\uparrow}^{\text{eq}} + n_{i\downarrow}^{\text{eq}}$ for $V = 0.3$ are shown. A $2k_F$ oscillation in the charge distribution is induced by the boundaries.¹² For all i , $\langle n_i \rangle$ is almost unity as in the equilibrium case ($\langle n_i \rangle = n_i^{\text{eq}} = 1$ for $V = 0$). The electron density $\langle n_i \rangle$ is basically unchanged by the bias voltage V when J is small. The scalar potential ψ_i has a linear dependence on i as shown in the inset of Fig. 3(a). This is because the long-range interaction term in Eq. (6) is small for $\langle n_i \rangle \sim 1$, so that ψ_i is determined only by the boundary conditions. The “equilibrium” part n_i^{eq} , on the other hand, deviates from unity near the left and right electrodes, where the deviation is canceled by the “nonequilibrium” parts δn_i^α , as shown in Fig. 3(b). The quantity δn_i^L have nonnegative values for all i because electrons come in from the left electrode. Although δn_i^L is large near the left electrode, it decays as i increases. On the other hand, δn_i^R have nonpositive values for all i because electrons go out to the right electrode. Note that $\delta n_i^R = -\delta n_{L_C+1-i}^L$ for $\gamma_L = \gamma_R$, no work-function differences, and at half filling.¹² The behaviors of δn_i^L and δn_i^R indicate that electrons and holes hardly penetrate into the central part and the resistive state is maintained. The current hardly flows through the central part, be-

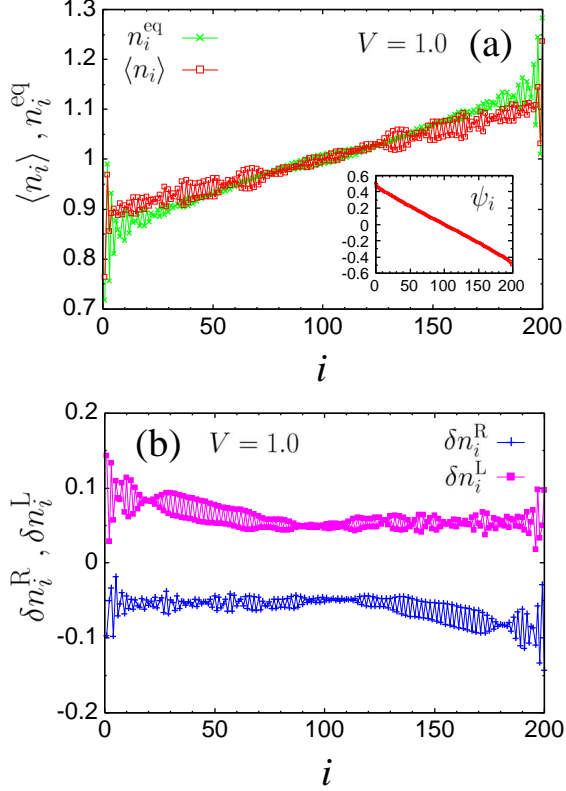


FIG. 4: (Color online) (a) Electron density, $\langle n_i \rangle$, “equilibrium” part, n_i^{eq} , and (b) “nonequilibrium” parts δn_i^{R} and δn_i^{L} for $\delta t = 0.025$, $L_C = 200$, $U = 0$, $V_p = 0.1$, $\gamma_L = \gamma_R = 0.1$, and $V = 1.0$. The scalar potential ψ_i is shown in the inset of (a).

cause J in Eq. (18) is determined by the difference between the density modulation by the left electrode at the right boundary, $\delta n_{i_R}^{\text{L}}$, and that by the right electrode at the left boundary, $\delta n_{i_L}^{\text{R}}$. Both terms $\delta n_{i_L}^{\text{R}}$ and $\delta n_{i_R}^{\text{L}}$ are vanishingly small, as shown in Fig. 3(b).

The charge distribution for $V = 1.0$, where the system is conductive, is qualitatively different from that for $V = 0.3$ as shown in Fig. 4. The spatial dependences of n_i^{eq} and $\langle n_i \rangle$ are nearly the same. They increase almost linearly from left to right except in the vicinities of the electrodes, where some oscillatory structure appears. The distributions of n_i^{eq} and $\langle n_i \rangle$ are understood by that of ψ_i shown in the inset of Fig. 4(a). The electron density is higher (lower) on the right (left) half where ψ_i is low (high). This behavior is caused by the electrons that move through the system in the conductive phase. The profile of ψ_i shows almost a linear dependence on i although a small deviation from the linearity near the electrodes is visible in contrast to the resistive phase, which is because the charge redistribution ($\langle n_i \rangle \neq 1$) is easier in the conductive phase. As for the “nonequilibrium” parts of the density shown in Fig. 4(b), δn_i^{L} have positive values for all i , while δn_i^{R} are negative for all i because the electrons come in from the left electrode

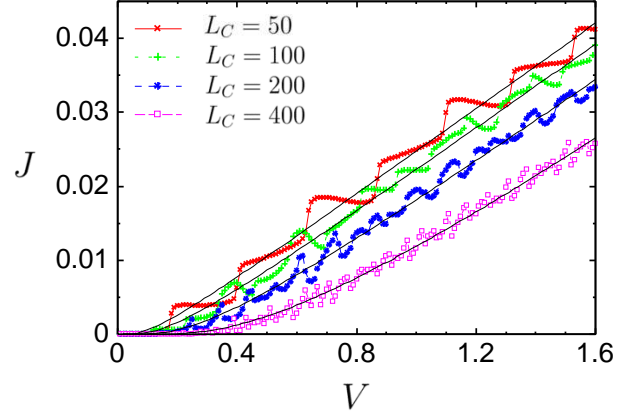


FIG. 5: (Color online) I - V characteristics of one-dimensional band insulators for several values of L_C with $\delta t = 0.025$, $U = 0$, $V_p = 0.1$, and $\gamma_L = \gamma_R = 0.1$. The solid lines show the function $J = aVe^{-V_{\text{th}}/V}$ which fits to the results.

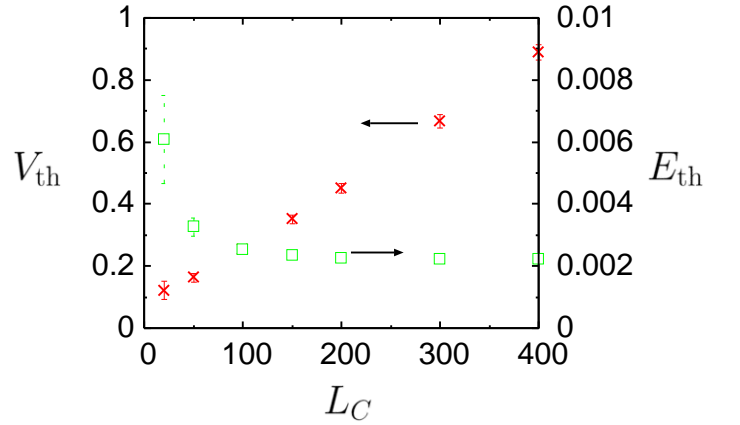


FIG. 6: (Color online) Dependence of the threshold bias voltage V_{th} and the threshold electric field E_{th} on the size of the central part L_C . The other parameters are the same as in Fig. 5. The error bars in the fitting are also shown.

and go out to the right electrode. A finite current flows through the central part: $\delta n_{i_R}^{\text{L}}$ and $\delta n_{i_L}^{\text{R}}$ are finite and have the opposite signs.

Next, we discuss the breakdown mechanism of band insulators. In Fig. 5, we show the I - V curves for different sizes of the central parts L_C with $\delta t = 0.025$. To the numerical results, the function,

$$J = aVe^{-V_{\text{th}}/V}, \quad (19)$$

is well fitted, where a and V_{th} are parameters. This expression originates from the LZ tunneling mechanism through which the insulator breaks down with the threshold voltage V_{th} .¹⁴ For $V < V_{\text{th}}$, the current J is exponentially suppressed due to the energy gap, while it increases linearly for $V > V_{\text{th}}$. When the central part is large, the fitting works well as shown in Fig. 5, so that the breakdown is consistent with the LZ tunneling

picture, although there exist fine structures in the I - V characteristics which come from the discreteness of the energy spectrum of the central part. As L_C decreases, the structure becomes more prominent. For $L_C = 50$, for example, a deviation from the fitting curve due to the stepwise structure becomes large, which indicates the LZ mechanism is no longer applicable to small- L_C systems.

Figure 6 shows V_{th} determined by fitting Eq. (19) to the data for each L_C , together with the corresponding electric field $E_{th} \equiv V_{th}/L_C$. For large L_C , V_{th} is proportional to L_C , so that E_{th} becomes a constant. In band insulators, the LZ breakdown is known to be induced by the applied electric field.^{23,24} Since the one-particle picture holds in band insulators, this breakdown can be analyzed as a usual interband tunneling problem and the threshold electric field becomes $E_{th} \propto \Delta^2/W$.³¹ The breakdown occurs when the energy gain by displacing an electron with charge $-e$ in an electric field E by the distance $\xi = W/\Delta$, $eE\xi$, overcomes the energy gap Δ . Here, $W \simeq 4$ is the bandwidth and $\xi \sim 40$. We have obtained the threshold $E_{th} = 0.0022$, which is comparable with the value obtained by the LZ formula,^{23,24} $(\Delta/2)^2/v = 0.00125$ with $v = 2$. In short, the threshold is governed by the electric field.

When the central part is small, the fitting to the I - V curve becomes worse because the finite-size effect becomes severe. The LZ mechanism is not suitable for understanding this breakdown. In this case, another mechanism, in which the threshold is determined by the bias voltage, is more appropriate for the following reason. As L_C decreases, it eventually becomes smaller than the correlation length ξ . The tunneling occurs when the energy gain by displacing an electron by the distance L_C , eEL_C , overcomes the energy gap Δ . This indicates that the mechanism of the breakdown continuously changes around $L_C \sim \xi$ as a function of L_C . When V exceeds Δ , some energy levels of the central part come in between μ_L and μ_R . For $L_C < \xi$, the wave functions do not fully decay in the system: the electron injected from the left electrode with energy higher than $\Delta/2$ can reach the right electrode through these levels so that the current flows. This can be clearly seen in Fig. 5 for $L_C = 50$ where the gap is $\Delta \sim 0.2$ due to the finite-size effect. The I - V curve shows an abrupt increase at $V \sim \Delta$ because μ_L exceeds the lowest unoccupied energy level of the central part. Each stepwise increase in the I - V characteristics corresponds to the increase in the number of energy levels located between μ_L and μ_R .

We have numerically confirmed that the results are qualitatively unchanged even if the long-range Coulomb interaction strength V_p and the system-electrode coupling strength γ_L ($= \gamma_R$) are varied. Thus, the threshold shows a crossover as a function of L_C . When $L_C > \xi$, the LZ-type breakdown occurs and the threshold is governed by the electric field. For $L_C < \xi$, on the other hand, the current flows when V exceeds the energy gap Δ .

It is noted that the spatial dependence of ψ_i is important for the realization of the field-induced breakdown as

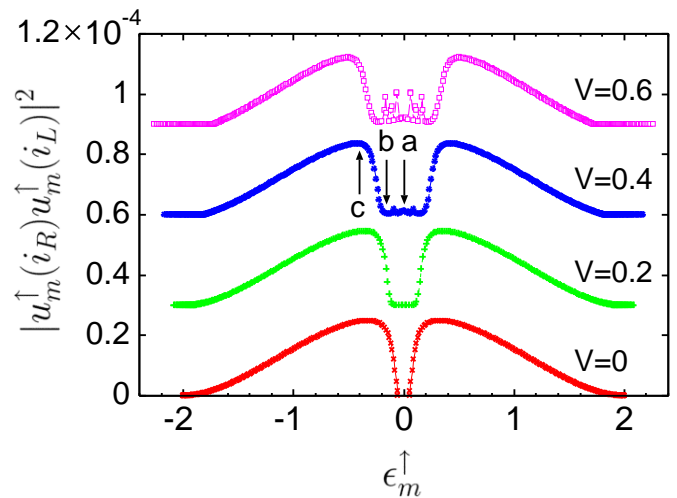


FIG. 7: (Color online) $|u_m^\sigma(i_R)u_m^\sigma(i_L)|^2$ with $\sigma = \uparrow$ plotted against ϵ_m^\uparrow for $V = 0, 0.2, 0.4$, and 0.6 in the case of $\delta t = 0.025$, $L_C = 400$, $U = 0$, $V_p = 0.1$, and $\gamma_L = \gamma_R = 0.1$. For $V = 0.2, 0.4$, and 0.6 , the lines are shifted upward by $0.3, 0.6$, and 0.9 , respectively.

well as the spatial modulation of the wave functions as discussed below. For small V , ψ_i has a linear dependence on i throughout the central part because the electrons are localized, $\langle n_i \rangle \simeq 1$, so that the effect of the long-range interaction on ψ_i is small. When the system is conductive, the charge redistribution occurs near the interfaces where a small deviation from the linearity is seen in ψ_i . This charge redistribution weakens the electric field on the sites away from the interfaces in the central part. For comparison, we show in the Appendix the I - V characteristics that are obtained by artificially setting $\psi_i = 0$ for all i . This corresponds to a hypothetical case where a sufficiently large charge redistribution occurs near the interfaces. There is no electric field in the central part: a voltage drop occurs only at the interfaces. In this extreme case, we obtain the threshold bias voltage $V_{th} \sim \Delta$ regardless of the length L_C , which is in contrast to the LZ-type behavior for large L_C in Fig. 6. Such a situation never occurs in our calculations with ψ_i and for realistic parameters. As we will discuss in the next section and also in the Appendix, the effect of the spatial profile of ψ_i on the breakdown mechanism of Mott insulators is basically the same as in the case of band insulators. Thus, the model without ψ_i is inappropriate for realistic insulators.

In discussing the breakdown for $L_C \gg \xi$, the spatial dependences of the wave functions $u_m^\sigma(i)$ are crucial as explained above. In Fig. 7, we show $|u_m^\uparrow(i_R)u_m^\uparrow(i_L)|^2$ as a function of the real part of the one-particle energy ϵ_m^\uparrow for several values of V in the case of $L_C = 400$. The behavior of this quantity for $\sigma = \downarrow$ is the same. It shows whether a given one-particle state contributes to the current J . Note that J is obtained by integrating $||G_\sigma^r(\epsilon)||_{i_L i_R}|^2$ over $\mu_R < \epsilon < \mu_L$. Since $\epsilon - \epsilon_m^\sigma$ ap-

pears in the denominator for $[G_\sigma^r(\epsilon)]_{ij}$ [Eq. (8)], the one-particle state m with finite $|u_m^\sigma(i_R)u_m^\sigma(i_L)|^2$ in the interval $-V/2 = \mu_R < \epsilon_m^\sigma < \mu_L = V/2$ gives a large contribution to J . This quantity directly shows whether the one-particle state m is localized or delocalized because it comes from the product of the amplitudes of the wave function at the two interfaces i_L and i_R . If $|u_m^\sigma(i_R)u_m^\sigma(i_L)|^2$ is large, the state has finite amplitudes at both sides of the central part, so that it is delocalized. If $|u_m^\sigma(i_R)u_m^\sigma(i_L)|^2$ is small, on the other hand, the state has a small amplitude at either of the interfaces.

For $V = 0$, $|u_m^\uparrow(i_R)u_m^\uparrow(i_L)|^2$ shows two bands that correspond to the conduction and valence bands in the band insulator. Because of the energy gap, no state exists in the region $-\Delta/2 < \epsilon_m^\sigma < \Delta/2$ for $V = 0$ so that the current does not flow at least for $V < \Delta$. When $V = 0.2$, several states appear in the region $-\Delta/2 < \epsilon_m^\uparrow < \Delta/2$, corresponding to the leakage of one-particle states from the electrodes to the central part. However, these states do not contribute to the current because their $|u_m^\uparrow(i_R)u_m^\uparrow(i_L)|^2$ are vanishingly small as shown in Fig. 7. Note that the line for each $V \neq 0$ is shifted upward by $\frac{3}{2}V$. For $V = 0.4$, the number of states around $\epsilon_m^\uparrow = 0$ with small $|u_m^\uparrow(i_R)u_m^\uparrow(i_L)|^2$ increases. The energy range where these localized states appear becomes wider as V increases. Consequently, the delocalized states that contribute to the current depart from the region $\mu_R < \epsilon < \mu_L$. Therefore, the current does not flow even if V barely exceeds the gap. As we show in the Appendix, the localized states do not appear if we set $\psi_i = 0$ for all i . It is crucial to take the spatial dependence of ψ_i into account to obtain the modulation of the wave functions.

Figure 8 shows the spatial dependences of the squares of the absolute values of the wave functions $|u_m^\uparrow(i)|^2$ for $V = 0.4$ and several m whose ϵ_m^\uparrow are located at the positions indicated by the arrows in Fig. 7. Here m is so labeled that $\epsilon_m^\sigma < \epsilon_{m'}^\sigma$ for $1 \leq m < m' \leq L_C = 400$. Figure 8(a) shows the one-particle state in the lower band with $\epsilon_m^\uparrow = 0.0348$ ($m = 201$) which is inside the gap for $V = 0$. This state is localized on the left half of the central part. The reason is as follows. The scalar potential is high (low) near the left (right) electrode. Within each of the conduction and valence bands, the state whose weight is large near the left (right) electrode has a higher (lower) energy than others. In the present case, the indexes m for the valence band are $m = 206, 203, 201, 199, \dots, 3, 2, 1$, while those for the conduction band are $m = 195, 198, 200, 202, \dots, 398, 399, 400$. As m is lowered, the wave function of the one-particle state is generally extended to a wider region and its largest amplitude is shifted to the right, as shown in Fig. 8(b) for the case of $\epsilon_m^\uparrow = -0.157$ ($m = 191$). As m is lowered further, e.g., for $\epsilon_m^\uparrow = -0.400$ ($m = 175$) in Fig. 8(c), the one-particle state is delocalized to reach the right electrode. Then, its wave function has large amplitudes near both electrodes.

In order to overview the behaviors of the one-particle states, we show the contour map of one-particle states

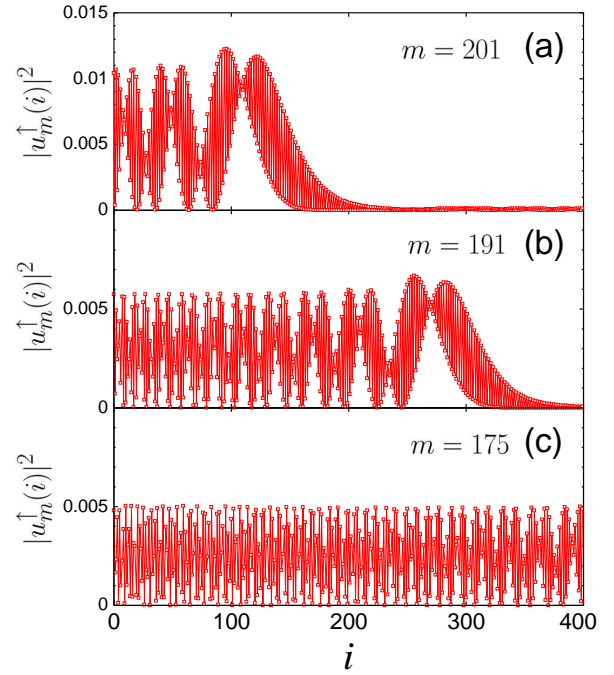


FIG. 8: (Color online) Spatial dependence of one-particle states $|u_m^\uparrow(i)|^2$ for (a) $m = 201$, (b) $m = 191$, and (c) $m = 175$ in the case of $V = 0.4$. The other parameters are the same as in Fig. 7. The corresponding ϵ_m^\uparrow are indicated by the arrows in Fig. 7.

$|u_m^\uparrow(i)|^2$ on the (i, m) plane for $V = 0.4$ in Fig. 9. For $V = 0.4$, the states $190 \lesssim m \lesssim 200$ are localized near the left electrode, and the states below are delocalized. At the bottom of the lower band, the states are localized near the right electrode because of the low scalar potential near the right electrode.

B. Mott insulators

In this section, we consider the case where the central part is described by the Hubbard model. Figure 10 shows the I - V characteristics for $\delta t = 0$, $L_C = 200$, $U = 1.5$, $V_p = 0.1$, and $\gamma_L = \gamma_R = 0.1$. When $V = 0$, the system is an antiferromagnetic insulator owing to the Hartree-Fock approximation. The energy gap Δ is then 0.25. In the previous studies on the I - V characteristics of metal-Mott-insulator interfaces,^{10,11} the current was calculated by solving the time-dependent Schrödinger equation. It is argued that the results obtained by the time-dependent Hartree-Fock approximation for the electron-electron interaction are consistent with those obtained by exact many-electron wave functions on small systems. For example, the suppression of rectification at metal-Mott-insulator interfaces is described by both methods.¹¹ Although the present time-independent Hartree-Fock approximation is worse, we expect the present approach captures the essential features of nonequilibrium steady

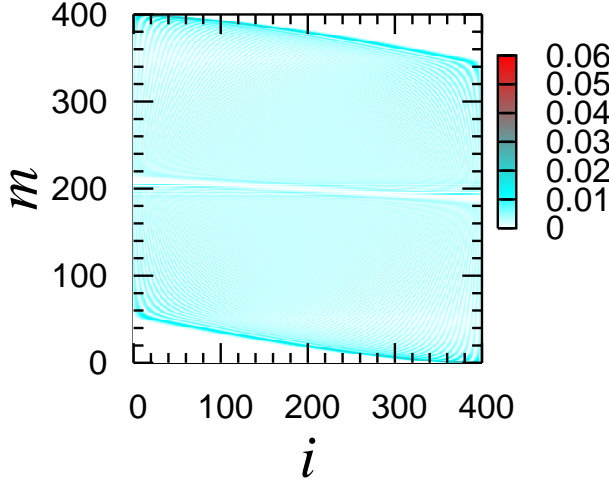


FIG. 9: (Color online) Contour map of one-particle states $|u_m^\uparrow(i)|^2$ in (i, m) plane for $V = 0.4$. The other parameters are the same as in Fig. 7.

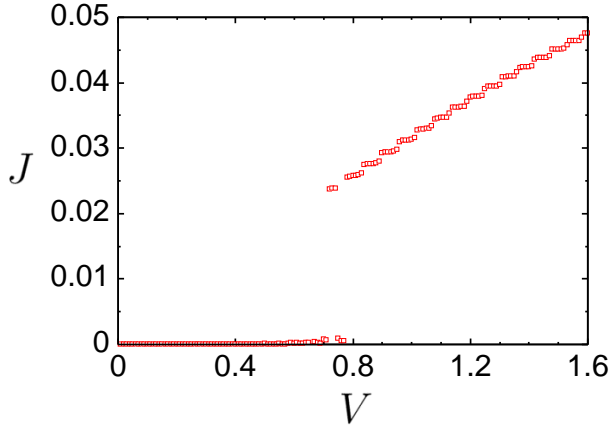


FIG. 10: (Color online) I - V characteristics of one-dimensional Hubbard model for $\delta t = 0$, $L_C = 200$, $U = 1.5$, $V_p = 0.1$, and $\gamma_L = \gamma_R = 0.1$.

states under the bias voltage. As we increase V , the current begins to flow at $V_{\text{th}} \sim 0.8$. The breakdown becomes a first-order transition due to the Hartree-Fock approximation, which is in contrast to the case of band insulators in the previous section.

The charge distributions in resistive and conductive phases at finite V are shown in Figs. 11 and 12, respectively. Their overall features are similar to those in band insulators. For all i and $V < V_{\text{th}}$, the electron density $\langle n_i \rangle$ is almost unity, which is basically the same as in the equilibrium case ($\langle n_i \rangle = n_i^{\text{eq}} = 1$ for $V = 0$). The scalar potential ψ_i has a linear dependence on i as shown in the inset of Fig. 11(a). As for the “nonequilibrium” parts, δn_i^L (δn_i^R) is large near the left (right) electrode and de-

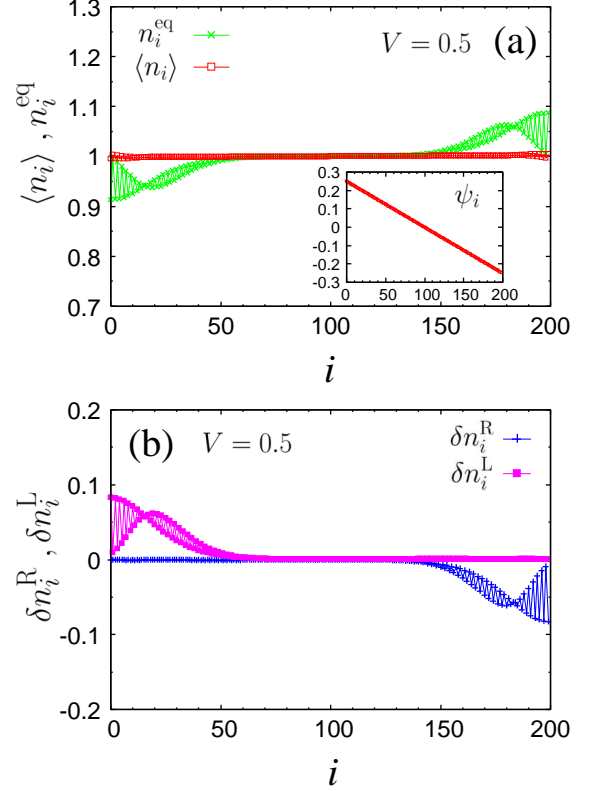


FIG. 11: (Color online) (a) Electron density, $\langle n_i \rangle$, “equilibrium” part, n_i^{eq} , and (b) “nonequilibrium” parts δn_i^R and δn_i^L for $\delta t = 0$, $L_C = 200$, $U = 1.5$, $V_p = 0.1$, $\gamma_L = \gamma_R = 0.1$, and $V = 0.5$. The scalar potential ψ_i is shown in the inset of (a).

cays as i increases (decreases) [Fig. 11(b)]. Electrons and holes do not penetrate into the central part so that the current does not flow.

For $V = 1.0 > V_{\text{th}}$, the spatial dependences of n_i^{eq} and $\langle n_i \rangle$ are shown in Fig. 12(a). They increase almost linearly from left to right. This reflects the profile of the scalar potential ψ_i that is higher (lower) on the left (right) half. The “nonequilibrium” parts of the densities, δn_i^L and δn_i^R are extended over the whole system with small spatial dependence [Fig. 12(b)],¹² which is in contrast to the resistive phase. Since $\delta n_{i_R}^L$ and $\delta n_{i_L}^R$ are finite with opposite signs, a finite current flows through the central part.

In Fig. 13, we show the threshold bias voltage V_{th} and the corresponding electric field $E_{\text{th}} = V_{\text{th}}/L_C$ for the first-order transition as a function of L_C . When the central part is small, i.e., $L_C \lesssim 50$, V_{th} is almost a constant near the energy gap $\Delta \simeq 0.25$. For small L_C , the electron injected from the left electrode with energy higher than $\Delta/2$ can reach the right electrode since the correlation length $\xi = W/\Delta \simeq 16$ is comparable to L_C . Thus, the threshold for $L_C < \xi$ is determined by the bias voltage. For $L_C \gg \xi$, on the other hand, V_{th} is proportional to L_C , so that the threshold is governed by the electric field. In recent theoretical studies,¹⁴ Oka and Aoki have

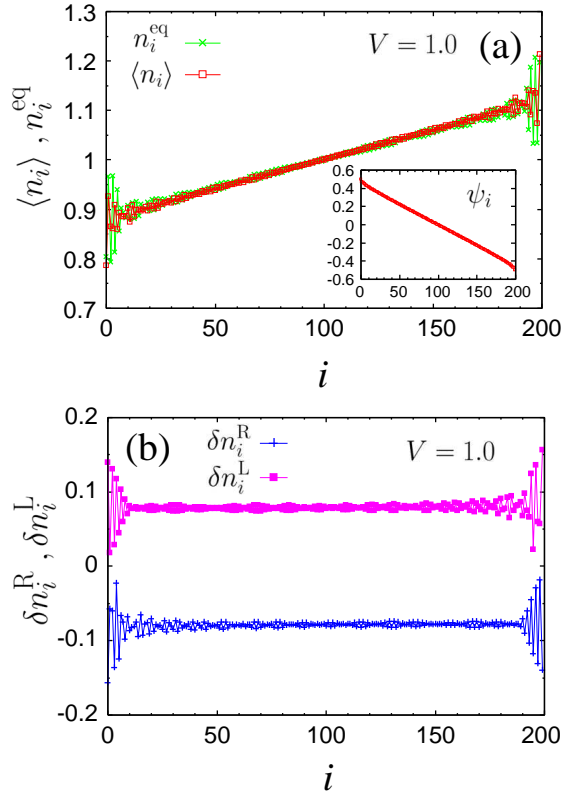


FIG. 12: (Color online) (a) Electron density, $\langle n_i \rangle$, “equilibrium” part, n_i^{eq} , and (b) “nonequilibrium” parts δn_i^{R} and δn_i^{L} for $\delta t = 0$, $L_C = 200$, $U = 1.5$, $V_p = 0.1$, $\gamma_L = \gamma_R = 0.1$, and $V = 1.0$. The scalar potential ψ_i is shown in the inset of (a).

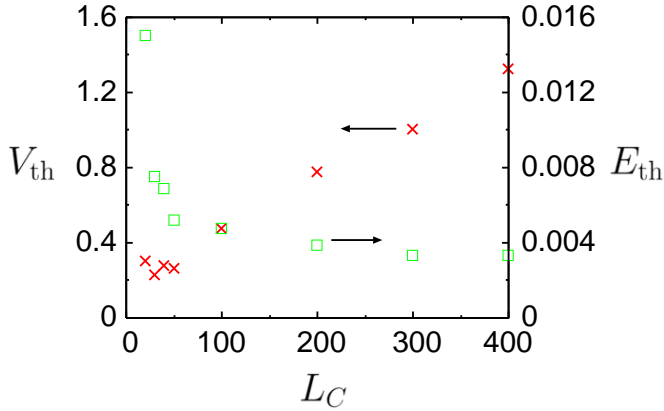


FIG. 13: (Color online) Dependence of the threshold bias voltage V_{th} and the threshold electric field E_{th} on the size of the central part L_C . The other parameters are the same as in Fig. 10.

proposed that the LZ breakdown occurs also in Mott insulators by applying the time-dependent density-matrix-renormalization-group method to the one-dimensional Hubbard model under an electric field with open boundary condition. In our calculations, the scalar potential ψ_i is linearly increasing with i in the resistive phase as

shown in Fig. 11 (a), which means that the electrons feel a uniform electric field in the central part. Therefore, our model describes the LZ breakdown as in the open Hubbard chain as long as the electrodes do not affect the nature of the breakdown for $L_C \gg \xi$. In fact, the threshold E_{th} is about 0.0033, which is comparable to the LZ value,¹⁴ $(\Delta/2)^2/v = 0.0078$, with $v = 2$. Thus, the threshold shows a crossover as a function of L_C as in the case of band insulators.

The LZ breakdown is explained as before by comparing the charge gap Δ and the work which is done by the electric field on an electron moving over the correlation length ξ . If the work $eE\xi$ exceeds Δ , the electron in the lower band may go over to the upper band so that the current flows. According to the results by Oka and Aoki,¹⁴ this consideration is applicable to Mott insulators where the correlation effects are important. Thus, we expect that the results obtained by the Hartree-Fock approximation are qualitatively unchanged even if we take account of the electron correlation. It is well known that the Hartree-Fock theory overestimates the charge gap Δ . It predicts the antiferromagnetic spin ordering which is actually destroyed if quantum fluctuations are appropriately taken into account. However, the overestimated Δ will alter the threshold only quantitatively. We also expect that the spin ordering does not essentially affect the breakdown itself since only the charge degrees of freedom are relevant to the mechanism. We note that the time-dependent density-matrix-renormalization-group method has been applied to a Mott insulator with electrodes very recently,³² and that the I - V characteristics have been consistently explained by the LZ tunneling mechanism. However, it is also shown that physical quantities such as the spin structure factor and the double occupancy do not reach a stationary state in the accessible time window. Therefore, a direct description of nonequilibrium steady states as in the present study is important to deepen our understanding of the breakdown.

Since the crossover behavior is obtained for both band and Mott insulators, the electron-electron interaction is not responsible for the phenomenon. We emphasize that the spatial profile of ψ_i is important for the realization of the LZ breakdown. In the Appendix, this is demonstrated for the Mott insulator by showing the I - V characteristics that are obtained by artificially setting $\psi_i = 0$ for all i . In this case, no electric field exists in the central part so that the modification of the wave functions does not occur. The I - V curves do not show any L_C dependence apart from the fine structures coming from the discreteness of the energy spectrum. We obtain the threshold bias voltage $V_{\text{th}} \sim \Delta$ regardless of the length L_C as in band insulators.

In Fig. 14, we show $|u_m^\dagger(i_R)u_m^\dagger(i_L)|^2$ as a function of the real part of the one-particle energy ϵ_m^\dagger for several values of V , where each line for $V \neq 0$ is shifted upward by V . The behavior of this quantity for $\sigma = \downarrow$ is the same. For $V = 0$, no state exists in the region $-\Delta/2 < \epsilon_m^\sigma < \Delta/2$ since the energy gap opens.

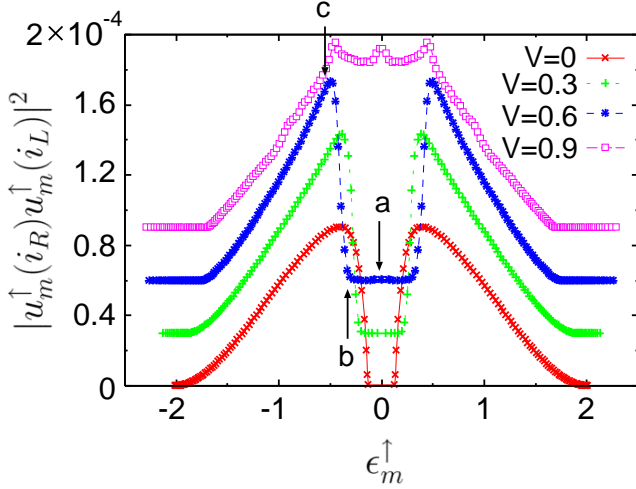


FIG. 14: (Color online) $|u_m^\sigma(i_R)u_m^\sigma(i_L)|^2$ with $\sigma = \uparrow$ plotted against ϵ_m^\uparrow for $V = 0, 0.3, 0.6$, and 0.9 in the case of $\delta t = 0$, $L_C = 200$, $U = 1.5$, $V_p = 0.1$, and $\gamma_L = \gamma_R = 0.1$. For $V = 0.3, 0.6$, and 0.9 , the lines are shifted upward by $0.3, 0.6$, and 0.9 , respectively.

$|u_m^\uparrow(i_R)u_m^\uparrow(i_L)|^2$ shows two bands that correspond to the upper and lower Hubbard bands. When $V = 0.3$, one-particle states leak from the electrodes to the central part so that several states appear in the region $-\Delta/2 < \epsilon_m^\uparrow < \Delta/2$. As in band insulators, these states do not have any contributions to the current because their $|u_m^\uparrow(i_R)u_m^\uparrow(i_L)|^2$ are vanishingly small. As we increase V further, e.g., $V = 0.6$, the states with vanishingly small $|u_m^\uparrow(i_R)u_m^\uparrow(i_L)|^2$ appear in a wider range around $\epsilon_m^\uparrow = 0$. The number of these localized states also increases. The appearance of the localized states keeps the central part resistive until V/L_C reaches the threshold electric field E_{th} even if $V > \Delta$ holds. When the system is conductive ($V > V_{th}$), the upper and lower Hubbard bands are merged into a single metallic band. In this case, all the states around $\epsilon_m^\uparrow \sim 0$ are delocalized and contribute to the current.

Figure 15 shows $|u_m^\uparrow(i)|^2$ as a function of i for $V = 0.6$. Here m is chosen at $100, 90$, and 85 , whose ϵ_m^\uparrow are located at the positions indicated by the arrows in Fig. 14. In Fig. 15(a), we show the wave function with $\epsilon_m^\uparrow = -0.00395$ ($m = 100$), which is localized on the left half of the central part. This state belongs to the lower Hubbard band. Since the scalar potential is high (low) near the left (right) electrode, the state is located near the top of the lower Hubbard band. The one-particle states in the band gradually lose their localized nature as m is lowered. This can be seen in Fig. 15(b) for the case of $\epsilon_m^\uparrow = -0.361$ ($m = 90$), where its largest amplitude is shifted to the right compared to that of $m = 100$. Figure 15(c) shows the one-particle state for $\epsilon_m^\uparrow = -0.497$ ($m = 85$), which is completely delocalized. Its wave function has large amplitudes near both electrodes. The spatial dependences of the one-particle states in the

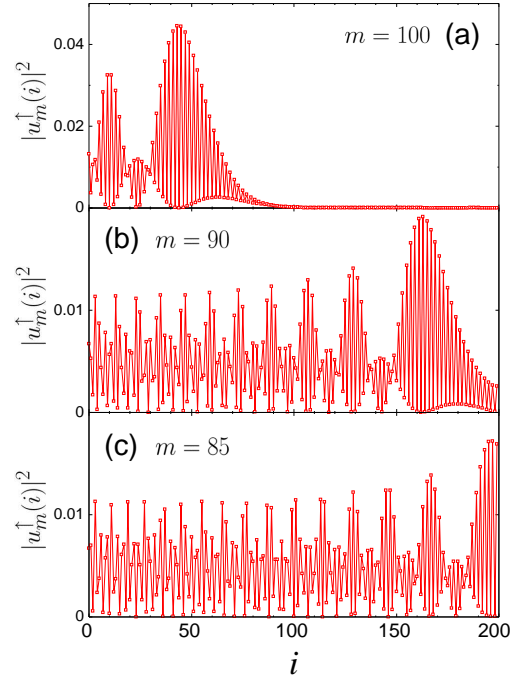


FIG. 15: (Color online) Spatial dependence of one-particle states $|u_m^\uparrow(i)|^2$ for (a) $m = 100$, (b) $m = 90$, and (c) $m = 85$ in the case of $V = 0.6$. The other parameters are the same as in Fig. 14. The corresponding ϵ_m^\uparrow are indicated by the arrows in Fig. 14.

resistive phase are similar to those in band insulators.

IV. SUMMARY

We have investigated the I - V characteristics of the one-dimensional band and Mott insulators attached to electrodes. A tight binding model with alternating transfer integrals for the band insulator and the Hubbard model for the Mott insulator are studied by using the nonequilibrium Green's function method. The applied bias voltage induces a breakdown of the insulating state to convert into a conductive state for both models. The threshold shows a crossover as a function of the size L_C of the insulators. For $L_C \lesssim \xi = W/\Delta$, the breakdown occurs at $V_{th} \sim \Delta$ so that the threshold is governed by the bias voltage. For $L_C \gg \xi$, the electric field determines the threshold, $V_{th}/L_C \propto \Delta^2/W$, which is consistent with the LZ breakdown reported previously.^{13,14} Since the crossover is obtained for both band and Mott insulators, the electron-electron interaction is not responsible for the phenomenon. The profile of the scalar potential ψ_i , which is linearly increasing with i in the resistive phase so that the electrons in the central part feel an almost uniform electric field, is important for the realization of the LZ breakdown and the crossover behavior.

Acknowledgments

This work was supported by Grants-in-Aid for Scientific Research (C) (Grant No. 19540381) and Scientific Research (B) (Grant No. 20340101), and by “Grand Challenges in Next-Generation Integrated Nanoscience” from the Ministry of Education, Culture, Sports, Science and Technology of Japan.

Appendix

In this appendix, we show the results when we artificially set $\psi_i = 0$ for all i . The I - V curves of the band insulator with $\delta t = 0.05$, $U = 0$, $\gamma_L = \gamma_R = 0.1$, and $\psi_i = 0$ for $L_C = 100, 200$, and 400 are shown in Fig. 16. It is apparent that the breakdown occurs at $V_{th} \sim \Delta$ regardless of the length L_C , which is consistent with Ajisaka *et al.*²² This is in contrast to the results in Fig. 6 where V_{th} is proportional to L_C for $L_C \gg \xi$.

When we fix $\psi_i = 0$, one-particle states do not leak

from the electrodes to the central part since the electric field is absent from the central part. In Fig. 17, we plot $|u_m^\dagger(i_R)u_m^\dagger(i_L)|^2$ as a function of ϵ_m^\dagger for several values of V . The results indicate that the one-particle energies and the wave functions are not affected by V . This comes from the fact that the Hamiltonian in Eq. (1) does not depend on $\langle n_i \rangle$ for band insulators if we set $\psi_i = 0$ for all i . Therefore, no localized state appears inside the gap for $V = 0$. In this case, the current begins to flow when V merely exceeds $V_{th} \sim \Delta$ since one-particle states with finite $|u_m^\dagger(i_R)u_m^\dagger(i_L)|^2$ appear in the region $\mu_R < \epsilon_m^\dagger < \mu_L$.

In Fig. 18, we show the I - V curves of the Mott insulator with $\delta t = 0$, $U = 1.5$, $\gamma_L = \gamma_R = 0.1$, and $\psi_i = 0$ for $L_C = 100, 200$, and 400 . As in the case of band-insulators, the breakdown occurs at $V_{th} \sim \Delta$ for all L_C . Although the breakdown seems to be continuous for $L_C = 100$ and 200 , a small discontinuity is evident for $L_C = 400$, which indicates a first-order transition. The discontinuity is more obvious for large U as shown in the inset of Fig. 18 for $U = 2$ with the gap $\Delta = 0.68$.

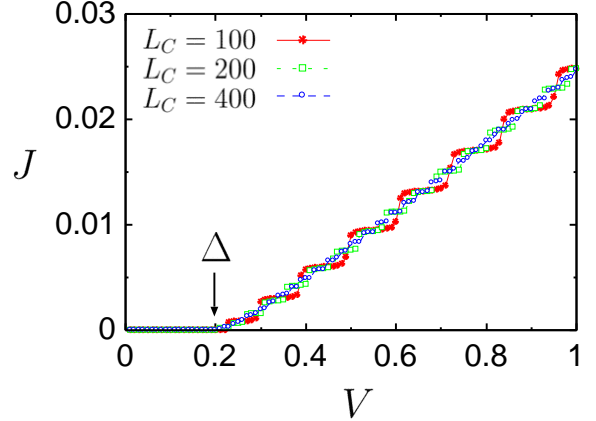


FIG. 16: (Color online) I - V characteristics in the case of $\delta t = 0.05$, $U = 0$, $\gamma_L = \gamma_R = 0.1$, and $\psi_i = 0$ for several values of L_C . The arrow indicates the location of the gap Δ .

* Electronic address: yasuihiro@ims.ac.jp

- ¹ Y. Taguchi, T. Matsumoto, and Y. Tokura, Phys. Rev. B **62**, 7015 (2000).
- ² R. Kumai, Y. Okimoto, and Y. Tokura, Science **284**, 1645 (1999).
- ³ S. Yamanouchi, Y. Taguchi, and Y. Tokura, Phys. Rev. Lett. **83**, 5555 (1999).
- ⁴ F. Sawano, I. Terasaki, H. Mori, T. Mori, M. Watanabe, N. Ikeda, Y. Nogami, and Y. Noda, Nature **437**, 522 (2005).
- ⁵ R. Kondo, M. Higa, and S. Kagoshima, J. Phys. Soc. Jpn. **76**, 033703 (2007).
- ⁶ S. Niizeki, F. Yoshikane, K. Kohno, K. Takahashi, H. Mori, Y. Bando, T. Kawamoto, and T. Mori, J. Phys. Soc. Jpn. **77**, 073710 (2008).
- ⁷ F. Sawano, T. Suko, T. S. Inada, S. Tasaki, I. Terasaki, H. Mori, T. Mori, Y. Nogami, N. Ikeda, M. Watanabe, and Y. Noda, J. Phys. Soc. Jpn. **78**, 024714 (2009).
- ⁸ T. S. Inada, I. Terasaki, H. Mori, and T. Mori, Phys. Rev. B **79**, 165102 (2009).
- ⁹ T. Hasegawa, K. Mattenberger, J. Takeya, and B. Batlogg, Phys. Rev. B **69**, 245115 (2004).
- ¹⁰ K. Yonemitsu, J. Phys. Soc. Jpn. **74**, 2544 (2005).
- ¹¹ K. Yonemitsu, N. Maeshima, and T. Hasegawa, Phys. Rev. B **76**, 235118 (2007).
- ¹² K. Yonemitsu, J. Phys. Soc. Jpn. **78**, 054705 (2009).
- ¹³ T. Oka, R. Arita, and H. Aoki, Phys. Rev. Lett. **91**, 066406 (2003).
- ¹⁴ T. Oka and H. Aoki, Phys. Rev. Lett. **95**, 137601 (2005).
- ¹⁵ T. Oka and N. Nagaosa, Phys. Rev. Lett. **95**, 266403 (2005).
- ¹⁶ T. Oka and H. Aoki, Phys. Rev. B **81**, 033103 (2010).
- ¹⁷ S. Onoda, N. Sugimoto, and N. Nagaosa, Prog. Theor. Phys. **116**, 61 (2006).
- ¹⁸ N. Sugimoto, S. Onoda, and N. Nagaosa, Prog. Theor. Phys. **117**, 415 (2007).
- ¹⁹ N. Sugimoto, S. Onoda, and N. Nagaosa, Phys. Rev. B **78**, 155104 (2008).

- ²⁰ S. Okamoto, Phys. Rev. B **76**, 035105 (2007).
- ²¹ S. Okamoto, Phys. Rev. Lett. **101**, 116807 (2008).
- ²² S. Ajisaka, H. Nishimura, S. Tasaki, and I. Terasaki, Prog. Theor. Phys. **121**, 1289 (2009).
- ²³ L. D. Landau, Phys. Z. Sowjetunion **2**, 46 (1932).
- ²⁴ C. Zener, Proc. R. Soc. London, Ser. A **137**, 696 (1932).
- ²⁵ S. Datta, *Quantum Transport: Atom to Transistor* (Cambridge University Press, Cambridge, 2005).
- ²⁶ Y. Tanaka and K. Yonemitsu, Physica B **405**, S211 (2010).
- ²⁷ Y. Meir and N. S. Wingreen, Phys. Rev. Lett. **68**, 2512 (1992).
- ²⁸ N. S. Wingreen, A.-P. Jauho, and Y. Meir, Phys. Rev. B **48**, 8487 (1993).
- ²⁹ A.-P. Jauho, N. S. Wingreen, and Y. Meir, Phys. Rev. B

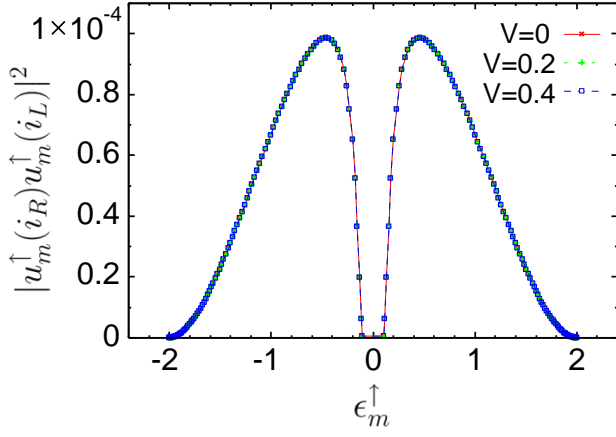


FIG. 17: (Color online) $|u_m^\sigma(i_R)u_m^\sigma(i_L)|^2$ with $\sigma = \uparrow$ plotted against ϵ_m^\uparrow for $V = 0, 0.2$, and 0.4 in the case of $L_C = 200$. The other parameters are the same as in Fig. 16.

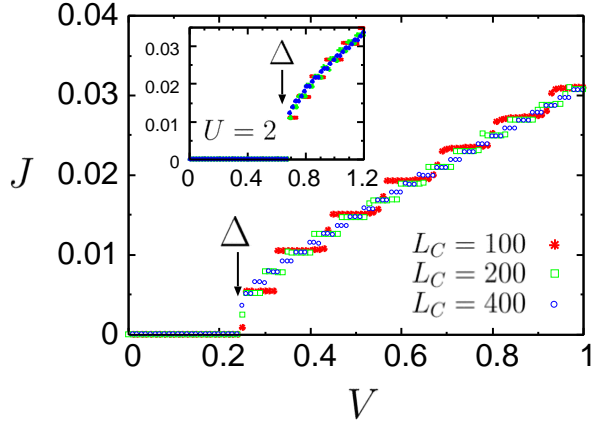


FIG. 18: (Color online) I - V characteristics in the case of $\delta t = 0$, $U = 1.5$, $\gamma_L = \gamma_R = 0.1$, and $\psi_i = 0$ for several values of L_C . The results for $U = 2$ and $\psi_i = 0$ are also shown in the inset. The arrow indicates the location of the gap Δ .

50, 5528 (1994).

³⁰ H. Haug and A.-P. Yauho, *Quantum Kinetics in Transport and Optics of Semiconductors* (Springer, Berlin, 2008) 2nd ed.

³¹ J. M. Ziman, *Principles of the Theory of Solids* (Cambridge University Press, Cambridge, 1979)

³² F. Heidrich-Meisner, I. González, K. A. Al-Hassanieh, A. E. Feiguin, M. J. Rozenberg, and E. Dagotto, Phys. Rev. B **82**, 205110 (2010).